

11 Electronics, DAQ, Controls, and Online Computing

This chapter describes the LZ signal processing electronics, data acquisition and trigger systems, detector-control system, and online data processing.

11.1 Signal Processing

The processing of the signals generated by the Xe PMTs is schematically shown in Figure 11.1.1. The Xe PMTs operate at a negative HV supplied by the LZ HV system, described in more detail in Section 11.7. HV filters are installed at the HV flange on the breakout box. The PMT signals leave the breakout box via a different flange and are processed by the analog front-end electronics, described in more detail in Section 11.3. The amplified and shaped signals are connected to the data acquisition (DAQ) and sparsification systems, described in more detail in Sections 11.5 and 11.6. The digitized data are sent to Data Collectors and stored on local disks.

The PMTs of the outer-detector system operate at positive voltage. The processing of the signals from these PMTs, shown schematically in Figure 11.1.2, is slightly different from the signal processing of the Xe PMTs shown in Figure 11.1.1. The HV filters of the outer-detector PMTs extract the PMT signals directly from the HV line; no separate signal flanges are required. The same type of amplifier used for the Xe PMTs is used for the outer-detector PMTs, except that only a single gain channel will be used to amplify and shape the outer-detector PMT signals.

The data flow is schematically shown in Figure 11.1.3. The event builder assembles the events by extracting the relevant information from the Data Collector disks, DAQ1–14. This step is discussed in more detail in Section 11.10. The event files are stored on local RAID arrays, RAID 1 and RAID 2, before being distributed to the data-processing centers for offline data processing and analysis.

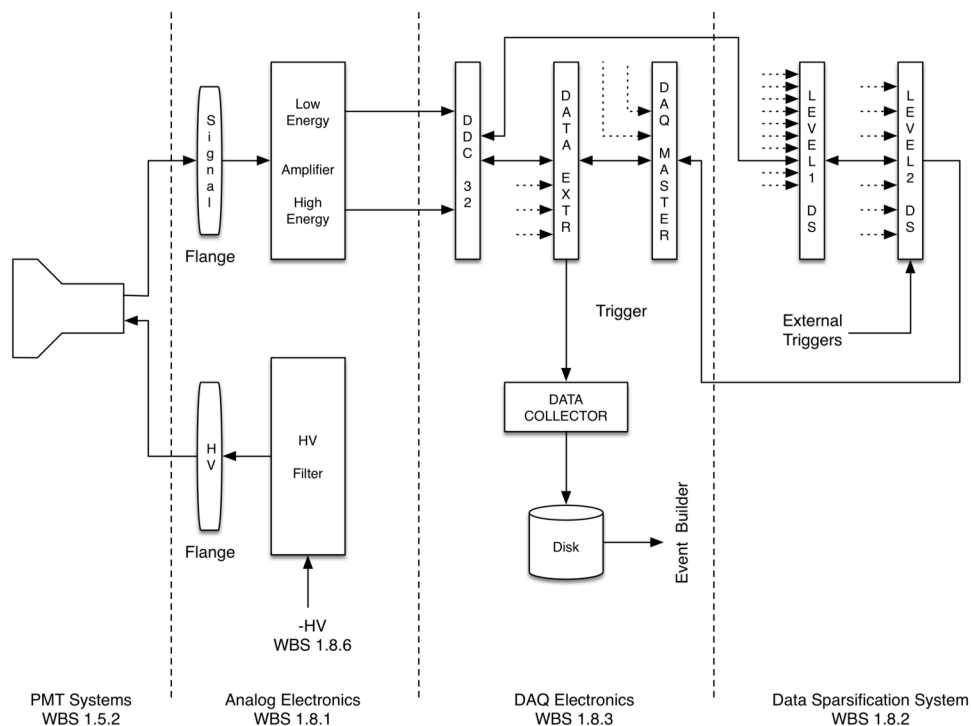


Figure 11.1.1. A schematic of the signal processing of the Xe PMTs. The PMTs of the TPC array use dual-gain signal processing. The PMTs of the skin PMTs only utilize the low-energy section of the amplifiers.

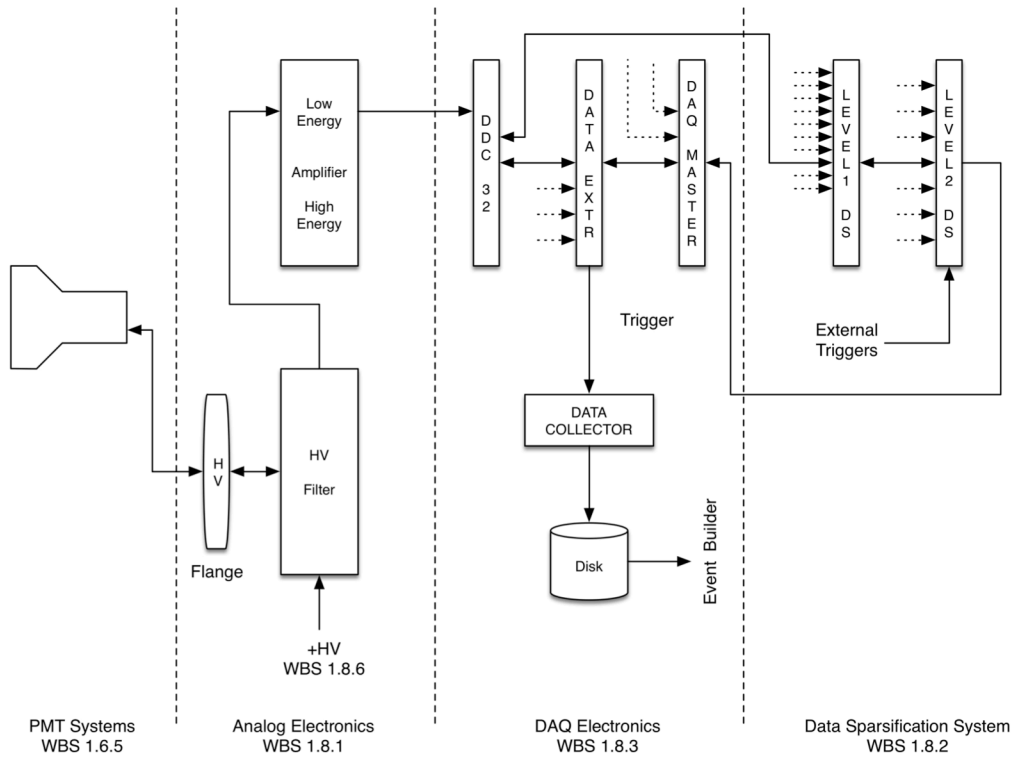


Figure 11.1.2. A schematic of the signal processing of the outer-detector PMTs.

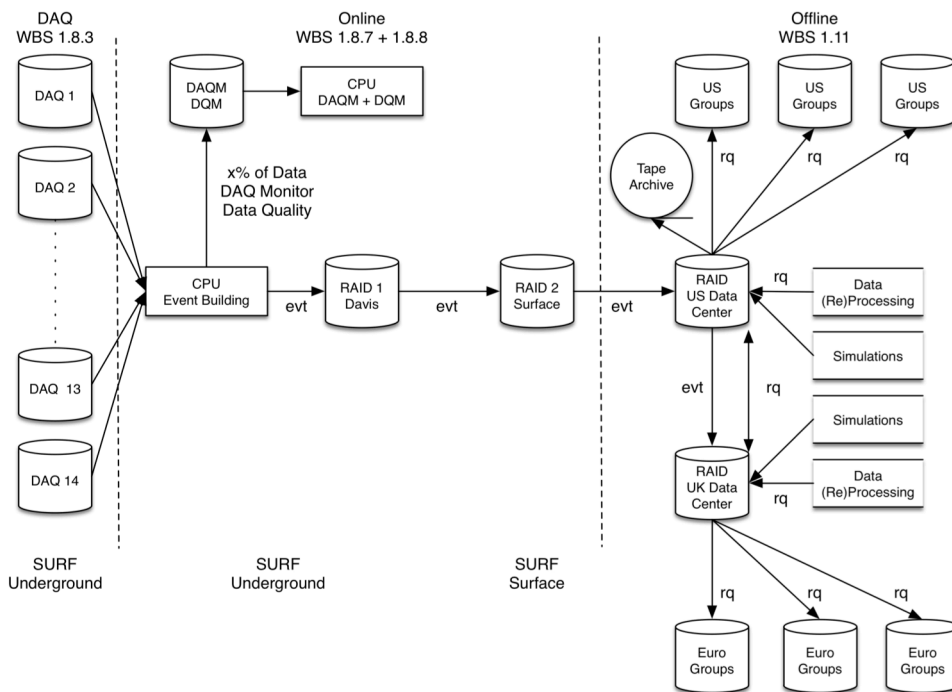


Figure 11.1.3. A schematic of the data flow.

11.2 Requirements

The parameters of the analog and digital electronics are defined based on the properties of the PMT signals, the required dynamic range of the different PMTs, and the expected calibration rates.

Three different PMTs are used in LZ. The TPC PMTs will see S1- and S2-type signals. The skin and outer-detector PMTs will only see S1-type signals. The relevant properties are listed in Table 11.2.1.

The cables that connect the Xe PMTs to the analog electronics are 40–60 ft long; the actual length depends on the final design of the conduits and the location of the area in which the analog electronics will be installed. These internal cables will be of the same type as those used for LUX. The manufacturer of the LUX cables (Gore) specifies an attenuation of 29 dB/100 ft at 400 MHz, similar to that of an RG178 cable. Measurements with the LUX cables have shown an amplitude reduction of S1 signals by approximately 30% for the 42-ft-long cables.

The design of the analog electronics is constrained by the required dynamic range of the LZ signals. Our design relies on the assumption that a single photoelectron (SPHE) detected in a TPC PMT generates a 13.3 mVns pulse at the input of the amplifiers. The required dynamic range is defined by the sources used to calibrate LZ and the desire to detect high-energy events for background studies. Chapter 10 provides details on the LZ calibrations.

The DAQ system design is based on our experience with LUX and the required LZ calibration rates. Typical calibration rates are listed in Table 11.2.2. The TPC source calibration rates are limited by the maximum drift time of 700 μ s in LZ. During source calibrations of the TPC, a 150 Hz calibration rate results in a 10% probability of detecting a second calibration event within the drift time of the previous calibration event. Neutron calibrations are carried out to define the NR band in the TPC. These calibrations utilize external neutron sources and a neutron generator. External sources, inserted into the source tubes around the central cryostat, are used to calibrate the skin and the outer-detector PMTs. The count rates for these calibrations are not limited by the drift time in the TPC and they can be carried out at substantially higher rates. Weekly LED calibrations are done to examine the SPHE response of the PMTs and to monitor the PMT response. These calibrations can be carried out with rates as high as 4 kHz.

The data volume to be handled by the DAQ system can be estimated on the basis of our experience with LUX. In WIMP search mode, we will focus on events with energy depositions below 40 keV. During krypton calibrations, in which the total energy deposition is 41.6 keV, the average LUX event size was 203 kB (or 1.7 kB/channel). The size of each event was dominated by the width of the S2 signals. The event size of LZ can be estimated by scaling the LUX event size by the ratio of the number of PMT

Table 11.2.1. Properties of the PMTs.

System	Type PMT	#	Gain	HV
TPC	R11410-20	488	$<5 \times 10^6$	<1500 V
Skin	R8520	180	$<1 \times 10^6$	<800 V
Outer detector	R5912	120	$<1 \times 10^7$	<1500 V

Table 11.2.2. Calibrations and expected count rates.

Calibration Type	System	Typical Count Rate	Frequency
Internal sources	TPC	<150 Hz	Twice a week (Kr)
External gamma sources	Skin and outer detector	TBD	TBD
Neutrons	TPC	<150 Hz	TBD
LEDs	TPC and outer detector	4 kHz	Weekly

channels. Because LZ has four times as many TPC PMTs as LUX, and taking into account the dual-gains, we expect that the event size in LZ will be roughly 8 times as large as the LUX event size, or 1.6 MB. This estimate does not include the data volume associated with the outer-detector and the skin PMTs. If each outer-detector and skin PMT detects a single S1-like pulse, that increases the event size by about 45 kB. With compression, the typical event size for LZ is estimated to be 0.53 MB. Monte Carlo simulations show that the total background rate in LZ will be about 40 Hz. The background rate in the WIMP search region (0–40 keV) will be about 0.4 Hz. At 40 Hz, the data rate is 21 MB/s. In 1,000 days, LZ will thus collect 1.9 PB of WIMP-search data. Other estimates, including energy depositions above 41.6 keV, result in an estimated total data volume of 2.8 PB. By optimizing the event selection, we expect to be able to reduce the total volume of WIMP-search data by a factor of 2 (see Section 11.6).

11.3 Analog Electronics

11.3.1 Design Criteria

The analog front-end design for the LZ experiment has benefited immensely from the experience with the LUX detector. In what follows, we have retained all the features of LUX electronics that performed well, improving some areas. The most important figure of merit of the LUX analog front end was its low noise characteristics, which allowed us to set our thresholds well below the SPHE level. Assuming the LZ noise characteristics are the same as those for LUX, we expect to be able to run with a threshold of 0.25 PHE (photoelectron) for each PMT. Figure 11.3.1.1 shows a simulated distribution of total S1 pulse area for events in which two PMTs detected one PHE each. A threshold of >0.25 PHE is set for each PMT. The distribution shown in Figure 11.3.1.1 is governed primarily by the $\sim 35\%$ rms width of the PMT signal, and receives almost no contribution from electronic noise. Setting a threshold at 1 PHE for the total S1 signal yields an efficiency of $\sim 95\%$ for events that produce at least two PHEs in the PMTs. It corresponds approximately to the *lowest* energy threshold achievable in such a detector, and hence drives the noise specifications for the front end.

The other key design parameter for the LZ front end is the dynamic range, defined by the sources used to calibrate LZ. Isotopes such as Kr-83m (32.1 and 9.4 keV transitions), activated Xe (236 keV and 164 keV transitions), and tritium (endpoint at 18.2 keV) will be present or injected directly into the LXe volume and will be used to calibrate the detector periodically. LZ will retain the ability to detect high-energy events that saturate the PMTs of the top array by using only the light collected by the bottom array to determine the total S2 area.

The LZ electronics will provide excellent resolution for single liquid electrons, which are expected to yield at most 50 PHEs, depending on the strength of the electric field in the gas region of the TPC. The typical duration of such pulses will be about 0.5–1 μ s. At the same time, we will need to provide extremely clean measurements of SPHEs in order to have a sharp turn-on of the S1 efficiency. SPHE spectra also help with maintaining an in situ calibration of the PMT gains. To meet these requirements, the analog electronics provides one low-energy (high-gain) and one high-energy (low-gain) output for each PMT.

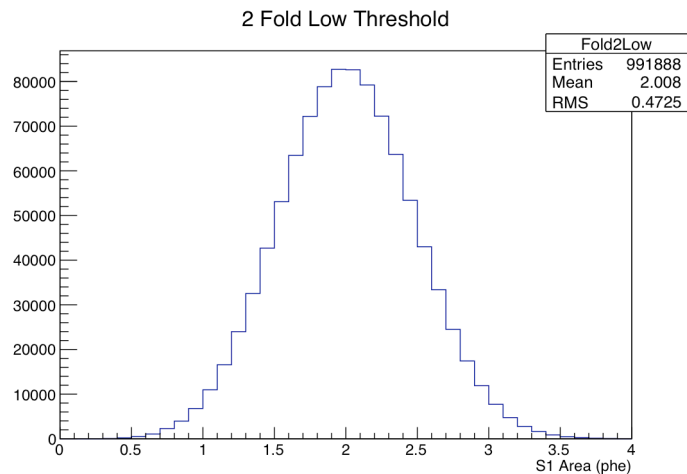


Figure 11.3.1.1. A simulated distribution of total pulse area for events in which two photoelectrons produce a signal >0.25 PHE in two PMTs.

Figure 11.3.1.2 shows this concept. The high-energy channel has low gain and a 30-ns full width at tenth maximum (FWTM) shaping-time constant. Its dynamic range is defined by the 236-keV Xe activation line. The low-energy channel has a 10× higher gain and wider shaping. It is optimized for excellent SPHE response and dynamic range. The shaping times and gains are derived from one assumption: the DAQ will have a usable dynamic range of 1.8 V at the input and will sample the pulses at 100 MHz with 14-bit accuracy. A 0.2 V offset is applied to the digitizer channels in order to measure signal undershoots of up to 0.2 V. Other relevant parameters are:

- SPHE response of the PMTs at the amplifier input: 13.3 mV-ns pulse.
- S1 light yield at 236 keV: between 1400 PHEs (for zero field) and 660 PHEs (for 1 kV/cm).
- S1 light distribution: evenly distributed over all PMTs. The bottom array receives 80% of the total S1 light.
- S2 light yield for ERs: 27 liquid electrons/keV and 50 PHEs/liquid electron (conservative maximum, assuming perfect liquid electron extraction).
- S2 light distribution: 22% of the S2 light is in a single top PMT. The S2 light is distributed evenly over all bottom PMTs; the bottom array receives 45% of the total S2 light.

The op-amps indicated in Figure 11.3.1.2 are very similar to those used in LUX. The gain and shaping-time constants of the

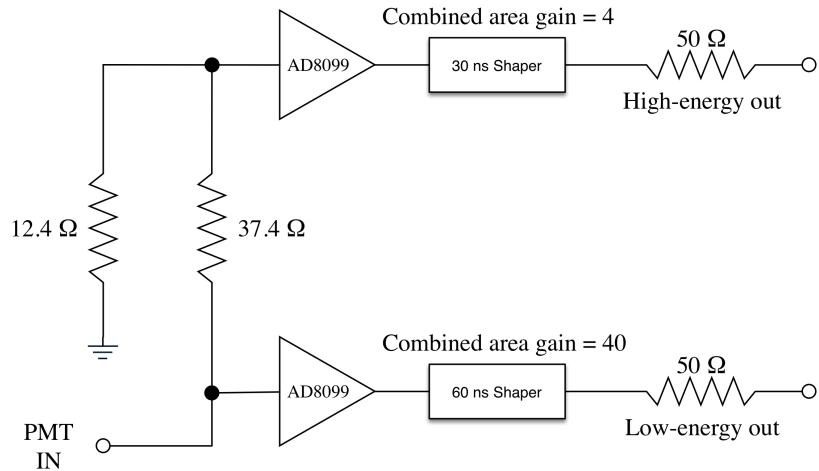


Figure 11.3.1.2. A schematic diagram of the LZ amplifier.

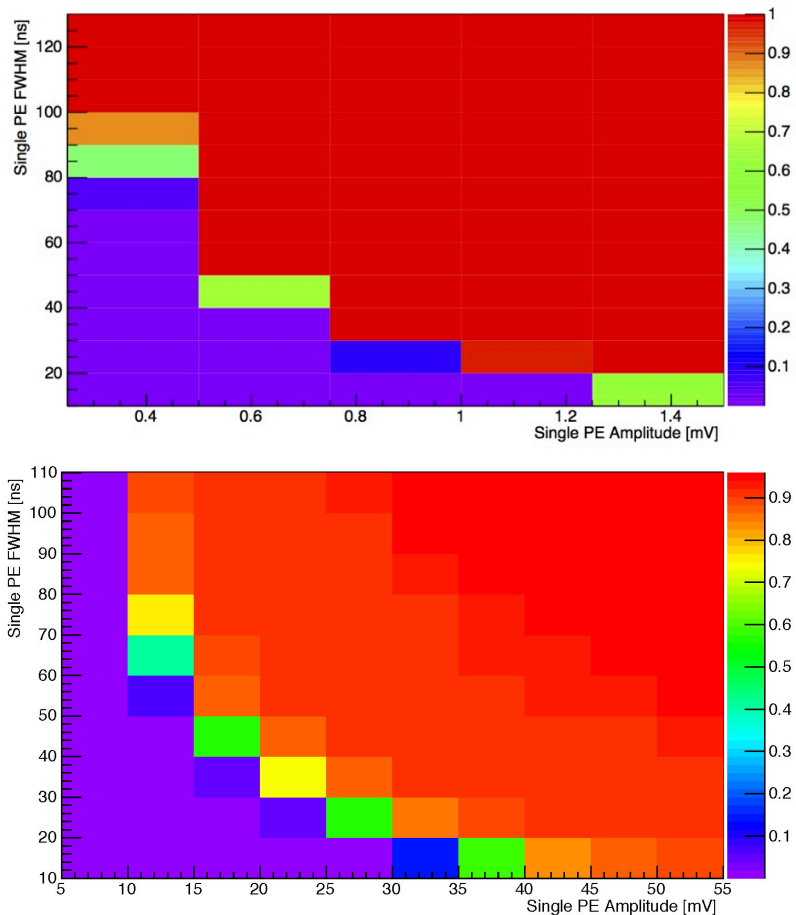


Figure 11.3.1.3. Top: A simulation study of the S2 response for a 236-keV Xe transition in the center of the detector, as seen by the top PMTs. The gain and the shaping width of the SPHE response are varied. The color code shows the fraction of events in which the peak PMT saturates. Bottom: A simulation study of the S2 response for a 3-MeV energy deposition in the center of the detector, as seen by the bottom PMTs. The color code shows the fraction of PMTs of the bottom array that saturate.

amplifiers were optimized using simulations. Figure 11.3.1.3 shows the results of simulations of S2 pulses associated with the 236-keV transition in activated Xe (top) and a 3-MeV energy deposition (bottom). Figure 11.3.1.3 (top) shows that S2 saturation in the top PMT array for the 236-keV transition is not a problem if the amplitude of a single PHE is less than 1.5 mV (12 ADCC). If we allow one PMT to saturate, single PHEs of up to 3.0 mV can be accommodated. Figure 11.3.1.3 (bottom) shows that the S2 associated with larger energy depositions will not start to saturate the PMTs of the bottom array if the amplitude of a single PHE is less than 15 mV (120 ADCC). The two outputs of the amplifiers have the following properties:

- **Low-energy output:** Gain 40, 1 PHE = 122 ADCC (amplitude), S1 dynamic range: 121 PHEs (4,600 keV), S2 dynamic range 14–31 keV (top) and 1,700–3,700 keV (bottom) for 0.5–1.1 μs wide pulses (1σ) with no saturation.
- **High-energy output:** Gain 4, 1 PHE = 24 ADCC (amplitude), S1 dynamic range: 600 PHEs, S2 dynamic range 140–310 keV (top) and 17,000–37,000 keV (bottom) for 0.5–1.1 μs wide pulses (1σ) with no saturation.

The dynamic range for S2 signals is shown in Figure 11.3.1.4. The low-energy channel of the amplifier provides the dynamic range required for the tritium and krypton calibrations. The high-energy channel is required to provide the dynamic range required to measure the activated Xe lines. S2 signals induced by alpha particles from radon decay will saturate one or more channels of the top array, but the S2 pulse area can still be reconstructed using the low-energy channels of the bottom PMTs.

The dynamic range for S1 signals is shown in Figure 11.3.1.5. The figure shows the dynamic range of a bottom PMT. Also shown are the number of PHEs associated with the full-energy deposition of the 236-keV Xe activation line and a 5.5-MeV alpha particle. The dynamic range provided by the dual-gain channels is sufficient for all LZ calibrations.

The final gain and shaping parameters of the amplifiers will be fixed after more detailed simulations, including the electronics response, have been carried out and the noise of all components of the

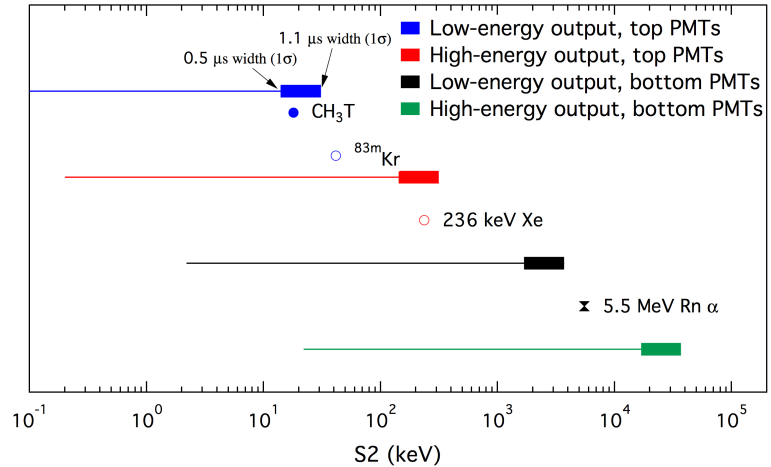


Figure 11.3.1.4. Dynamic range for S2 signals for the top and bottom PMTs. The bars indicate variations in the upper level of the dynamic range due to the variations in the width of the S2. The lower and upper ends of these bars show the dynamic range for 0.5- μs -wide and 1.1- μs -wide pulses, respectively.

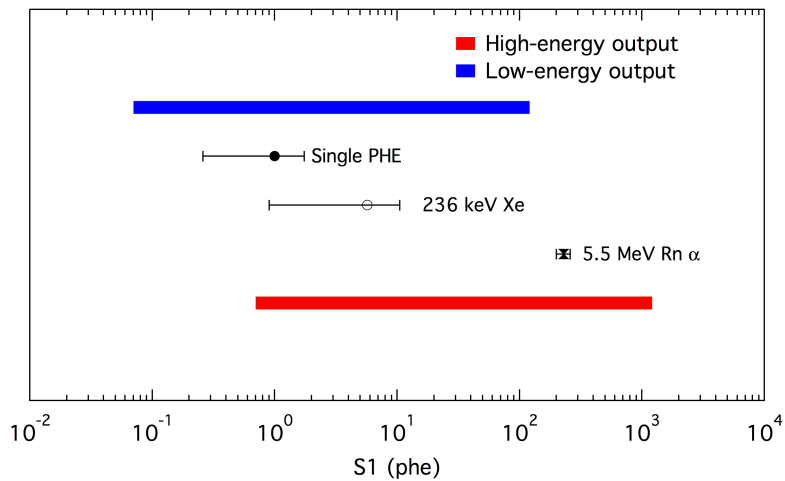


Figure 11.3.1.5. Dynamic range for S1 signals detected in the bottom PMTs. The range required for the Xe activation lines and alpha particles from radon decay are also shown.

Table 11.3.1.1. Summary of the number and type of the 1276 analog signals.

PMT Type	High-gain Signals			Low-gain Signals		
	#	Gain	Shaping (FWTM)	#	Gain	Shaping (FWTM)
Top TPC	247	40	60	247	4	30
Bottom TPC	241	40	60	241	4	30
Skin	180	TBD	TBD	0	NA	NA
Outer detector	120	TBD	TBD	0	NA	NA
Total	788			488		

electronics chain has been measured during a chain test.

The same amplifier design will be used for the skin and outer-detector PMTs although the gain and shaping may be adjusted. For these PMTs, only the low-energy channel will be instrumented. A summary of the number and type of analog signals is shown in Table 11.3.1.1.

11.3.2 LZ Amplifier Prototype

Figure 11.3.2.1 shows the first amplifier prototype with four input channels. The final amplifiers will have eight input channels. The amplifier will be installed on a signal flange and connected to the PMT signal lines using the DB-25 connector visible on the left side of the figure. The DB-25 connector allows the signal lines to be interleaved with two ground lines.

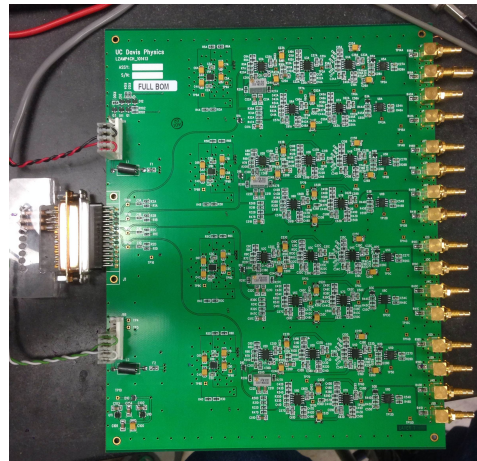


Figure 11.3.2.1. Photograph of the four-channel amplifier prototype. The input signals are connected to the DB-25 connector at the left side of the board. Each channel has four outputs, visible on the right.

A waveform captured with the pre-prototype of the digitizer is shown in Figure 11.3. 2.2. The digitizer captured the output of the low-gain channel of the amplifier when a 50 mV S1-like pulse was presented to the input of the amplifier.

The RMS ADC noise of the free-running digitizer channels was measured to be $1.19 \pm$

0.01 ADCC. When one of the low-gain channels of the amplifier, with the corresponding amplifier input terminated with 50Ω , was connected to the digitizer, the measured noise remained virtually unchanged (1.20 ± 0.01 ADCC). When one of the high-gain channels of the amplifier was connected, the measured noise increased to 1.58 ± 0.02 ADCC. The noise added by the high-gain channel was estimated to be 0.38 ± 0.02 ADCC ($46 \pm 2 \mu\text{V}$).

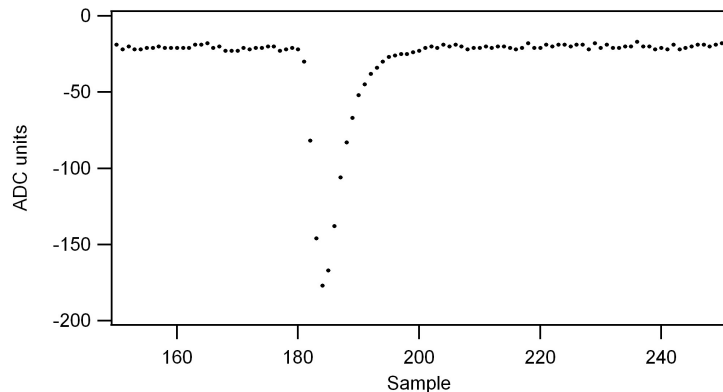


Figure 11.3.2.2. A waveform from the low-gain channel of the prototype LZ amplifier, captured with the pre-prototype of the LZ digitizer, sampling at 100 MHz. This waveform was generated when a 50 mV S1-like pulse was delivered to the input of the amplifier.

The crosstalk between the individual amplifier channels is shown in Figure 11.3.2.3. A pulse applied to the input produced a 1.2 V pulse at the high-gain

output (Ch 1). The associated low-gain signal is visible on Ch 2. Other channels show no evidence of crosstalk.

The linearity of the amplifier was studied using S1-like test pulses. The signals from the high-energy output saturate the dynamic range of the digitizers before nonlinear effects in the amplifier become important.

Examples of the results of these linearity studies with S1-like pulses are shown in Figure 11.3.2.4 The input pulses had a rise time of 18 ns and a fall time of 78 ns. The low-gain

output shows a linear behavior across the entire range of input signals used. The high-gain output becomes nonlinear when the area of the input signal exceeds 10 Vns. Although the response is nonlinear in this region, there is still a one-to-one correlation between the area of the digitized output pulse and the area of the input pulse.

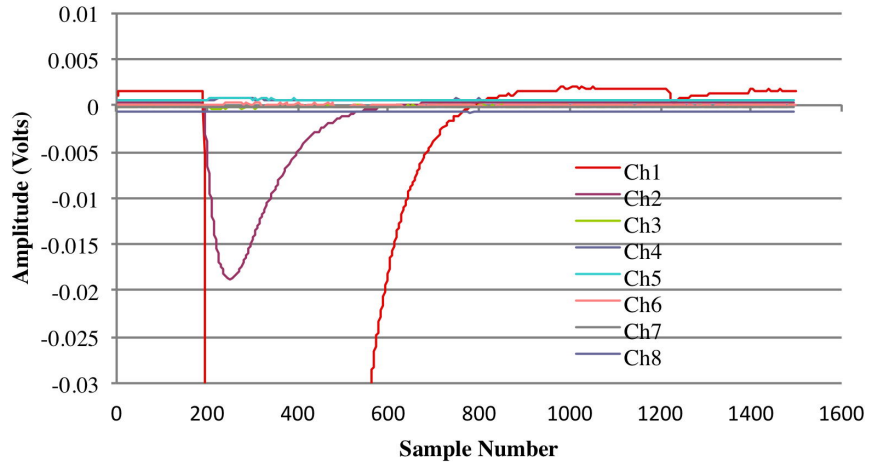


Figure 11.3.2.3. Output waveforms when a pulse on input 1 generates a 1.2 V output pulse on output 1.

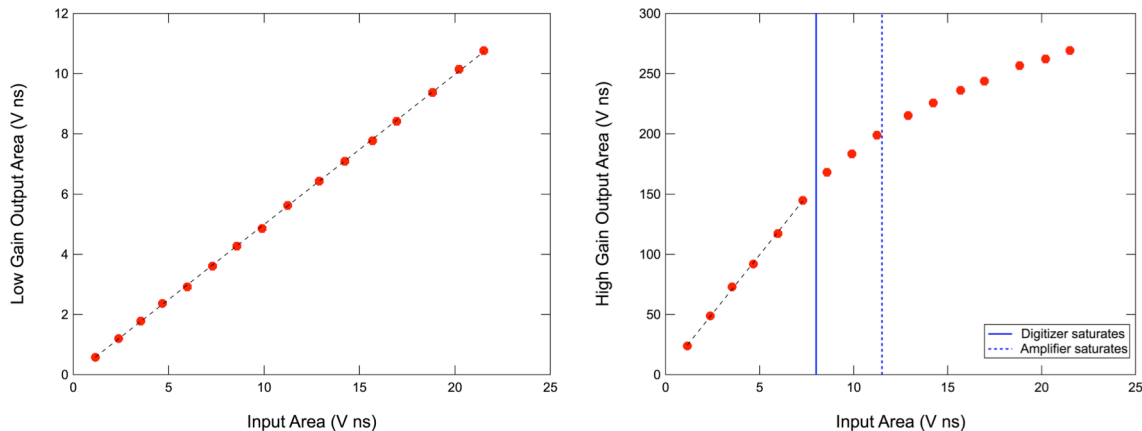


Figure 11.3.2.4. Results of linearity measurements. The area of the output pulse, captured with our digitizer, is plotted as function of the area on the input pulse. The results obtained for the low-gain (high-energy) channel are shown on the left while the data collected for the high-gain (low-energy) channel are shown on the right.

11.4 Digital Electronics

The LZ digital electronics is based on a digital platform (a motherboard); a prototype of this platform is shown in Figure 11.4.1. The final LZ motherboard will be based on this design, but will operate with a more powerful Kintex field-programmable gate array (FPGA) from Xilinx, either the new Series-7 or the newest UltraScale [1]. The final motherboard will provide gigabit Ethernet, RS-232, and low-voltage differential signaling (LVDS) interfaces, and four logic outputs, either TTL or NIM. Waveform memory (3,578 kB) will be provided by the FPGA. A large event-buffer memory of up to 128 MB will be provided by the dual-core processor. The onboard clock can be driven externally in order to synchronize multiple boards to the same clock source. Very high processing power, nominally 52 giga-operations per second, will be provided by the onboard FPGA. Two daughter card connectors can host two separate

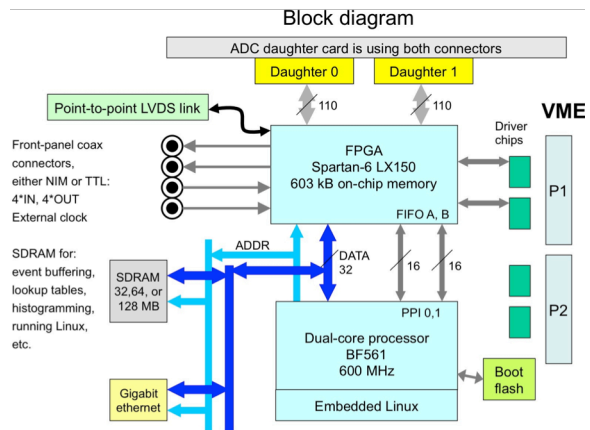
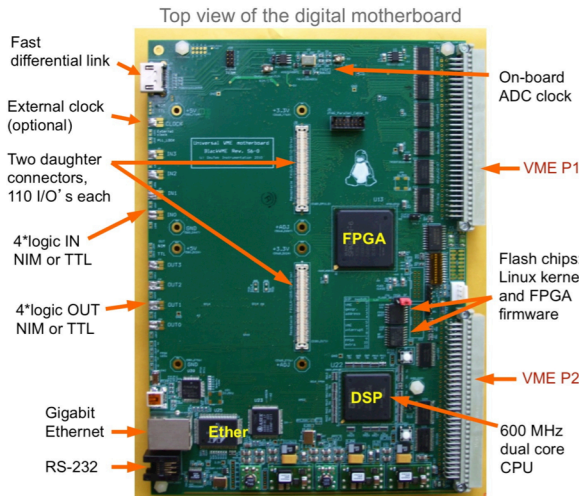


Figure 11.4.1. The digital motherboard used to develop the LZ digitizers. It provides gigabit Ethernet, RS-232, USB-2, VME, and LVDS interfaces. The FPGA and the dual-core processor are rated at 52 and 2.4 giga operations per second, respectively.

daughter cards, or one daughter card of twice the size. The I/O pins of these connectors are arranged as differential pairs, supporting either the differential or single-ended signals. A dual-core processor will be connected to the FPGA with the 32-bit memory bus, as well as two dedicated 16-bit-wide FIFOs. Readout of the FPGA data can be performed either via the memory bus or via the FIFOs, depending on the application. The board can be hosted in a 6U VME crate, or it can be powered with a tabletop power supply. Power consumption is minimized by using low-voltage chips.

The onboard processing power and multiple interfaces provide flexibility that can be applied to almost any project. The LVDS links enable custom communication architectures. The Ethernet provides support for distributed experiments and/or standalone remote applications. The processor is running Linux, which is popular, free, and fully customizable, allowing each board to perform on-the-fly data processing and online diagnostics.

The 32-channel ADC card shown in Figure 11.4.2 implements the digitizer front end. It provides 32 channels of digitization and two waveform reconstruction outputs for diagnostic. The ADC channels feature remote DC offset control. The card is connected to the two daughter connectors of the digital baseboard that provide the control signals and power. The printed circuit-board layout can accommodate quad A/D chips with sampling frequency up to 125 MHz. This card, installed on the digital motherboard, is referred to as the DDC-32 in the remainder of this chapter.

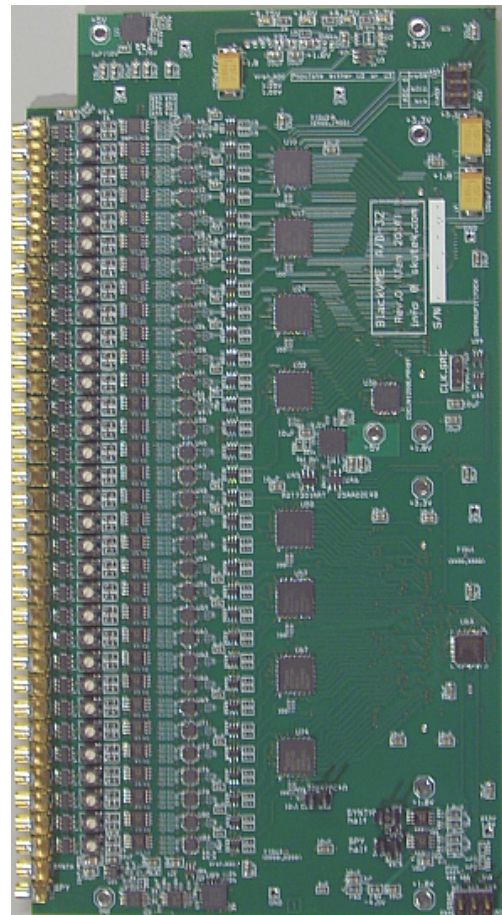


Figure 11.4.2. Prototype ADC daughter card with 32 channels.

11.5 DAQ

The top-level architecture of the LZ DAQ system is shown schematically in Figure 11.5.1. The DDC-32s continuously digitize the incoming PMT signals and store them in circular buffers. When an interesting event is detected, the Data Extractor (DE) collects the information of interest from the DDC-32s. The DEs compress and stack the extracted data using their FPGAs and send the data to Data Collectors (DCs) for temporary storage. The Event Builder (EB) takes the data organized by channels and assembles the buffers into full event structures for online and offline analysis. The DAQ operation is controlled by the DAQ Master (DM) for high-speed operations such as system synchronization and waveform selection, and by the DAQ Expert Control/Monitoring (DECM) system for slow operations such as running setup/control and operator diagnostics. The entire system runs synchronously with one global clock.

Figure 11.5.2 shows a more detailed overview of the different key elements of the DAQ system. The digitizers are sampling at 100 MHz with 14-bit resolution over a 2-V range. During normal operation, the boards will collect waveforms in a Pulse Only Digitization (POD) mode, which is expected to effectively reduce the raw waveform volume by a factor of 50 [2]. The amount of memory assigned to each channel is set so that no data truncation is expected even if the POD mode reduces the data volume by only a factor of 20. The POD waveforms are stored in dual-buffered memory that is divided into sections that hold the header information and the actual POD samples, as shown in Figure 11.5.3. Separate POD header and payload memories will improve the performance of extracting waveform data when the Data Sparsification Master (DSM) detects an event of interest [3].

The extreme flexibility that comes with using FPGAs and their internal memories allows us to assign the entire on-chip memory to just one specific channel when needed. This feature will be used for system diagnostics and noise measurements where capturing long, continuous (non-POD) waveforms is important. In such a mode, the DDC-32 will be able to capture 10-ms-long waveforms, suitable for power-spectral-density analysis.

The DEs and the DM use the same hardware but different firmware. They use the same motherboard as the digitizer boards, with different daughter cards that enable communication with multiple DDC modules and the DCs. Each daughter card can serve up to 12 DDC-32s over HDMI links and one DC over a

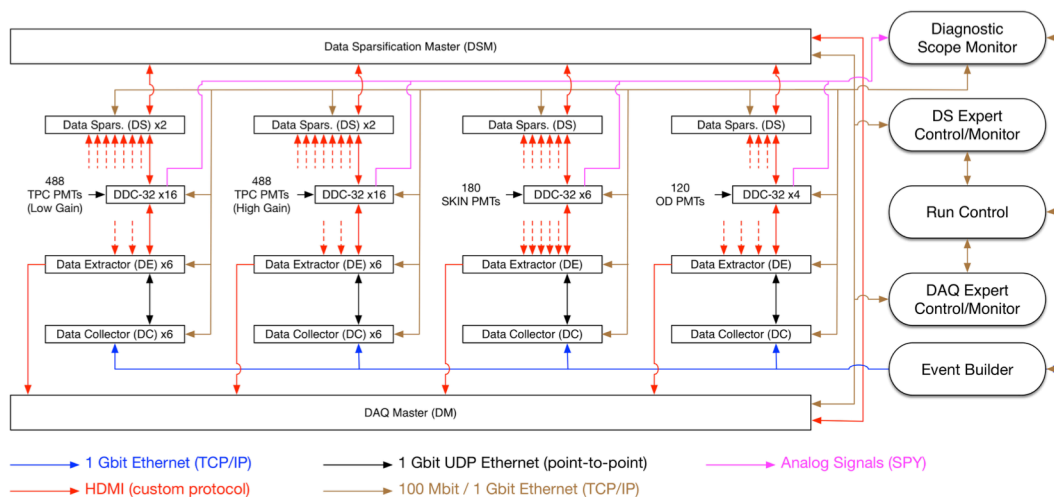


Figure 11.5.1. Diagram of the DAQ architecture. Groups of digitizers (DDC-32) capture the amplified and shaped signals from the Xe, skin, and outer-detector PMTs. The waveforms of interest are extracted from the DDC-32s and compressed by the Data Extractors (DEs) before they are passed to Data Collectors (DCs) for temporary storage. The DAQ Master Board (DM) coordinates the high-speed operation of the entire DAQ system when the Data Sparsification Master (DSM) signals the detection of waveforms to be preserved. The global clock distribution system is not shown in this diagram.

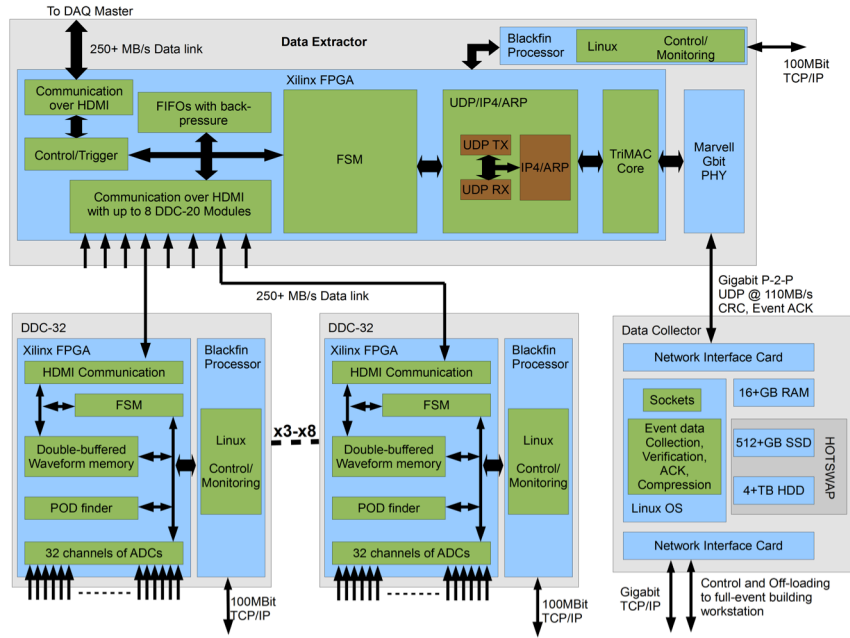


Figure 11.5.2. Detailed depiction of the inside of and interaction between the key elements of the proposed DAQ system.

dedicated gigabit Ethernet connection.

The HDMI link has seven single-ended lanes used for communicating states of the finite state machines (FSMs) between boards and four LVDS lanes used for fast offloading of the waveforms from the digitizers. On the current motherboard, we have used input/output serial/deserializer (IOSERDES) elements, offered in the Spartan-6 FPGA series, and have confirmed the advertised 1-Gbit throughput per LVDS lane.

The gigabit Ethernet link between the DE and the DC utilizes the User Datagram Protocol (UDP). To mitigate the limitations of UDP, we will add for each event a cyclic redundancy check (CRC) and acknowledgment, and also use the dedicated Ethernet link in a point-to-point topology to eliminate congestion and packet loss. All UDP packets formed by the DE's FPGA will be sent over a single gigabit Ethernet cable to a dedicated network port on the DC.

The DCs will be implemented using server-grade, rack-mountable (2U) workstations. We have tested a

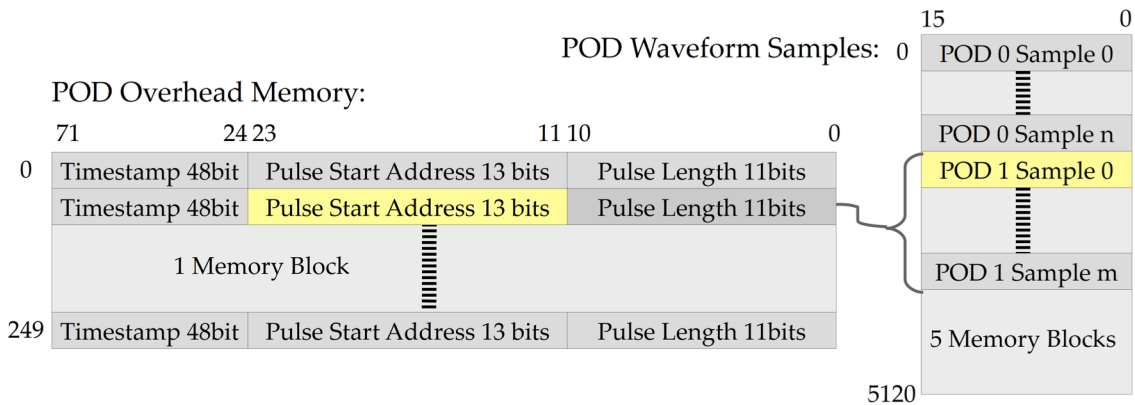


Figure 11.5.3. Depiction of the proposed memory organization of POD waveform storage in the FPGA for a single buffer (out of two) of a single channel. Separation of POD overhead and POD samples will improve the performance and ease of extracting information from memory.

Table 11.5.1. Key parameters of the prototype Data Collector.

Processor:	Intel Xeon E3-1270V3 3.5GHz Quad-Core	HDD:	SAMSUNG 840 Pro Series 256GB SSD
Motherboard:	ASUS P9D-V ATX		Western Digital RE 4TB 7200 RPM
Memory:	16GB Kingston DDR3 SDRAM ECC	Case:	NORCO RPC-270 2U Server Case
NIC:	Intel Ethernet Server Adapter I350-T2	Hot Swap:	ICY DOCK 3.5" and 2.5" SATAIII 6Gps HDD Rack Tray

Table 11.5.2. Summary of the performances of the DAQ links and their expected utilization levels.

Link	Expected Performance	Maximum Expected Usage	Usage
LVDS over HDMI	250+ MB/s	8.6 MB/s	< 3.5%
DE -> Gigabit UDP -> DC	109 MB/s	34.4 MB/s	< 33%

Table 11.5.3. Summary of the expected storage and buffering capabilities on the Data Collectors during calibrations.

Source	Data Rate per Data Collector (uncompressed)	512 GB Solid-state Drive		4 TB Hard-disk Drive	
		Raw	7z	Raw	7z
Kr-83	~5.2 MB/s	~1.1 days	~4.4 days	~9 days	~35 days
LED	~34.4 MB/s	~4 hours	~16 hours	~1.4 days	~5.3 days

prototype DC with the parameters shown in Table 11.5.1. We were able to confirm reliable data transfer from the DE to the solid-state drive (SSD) in the DC. With appropriate modifications to the network interface card (NIC) drivers, we were able to transfer data at a constant rate of 109.8 MB/s, with no data loss or corruption. Table 11.5.2 summarizes the tested link performances and their expected utilization.

The data stored on the DCs are processed by the Event Builder (EB). The EB builds events by sampling the different DC disks and collecting all information associated with a given event. The resulting event (EVT) files are compressed in order to achieve the smallest possible file size for storage and transmission. The EVT files are written to RAID array #1, located in the Davis Cavern, before being transferred to the RAID array #2, located on the surface at SURF. The RAID arrays have sufficient storage capacity for a full month of data taking.

The DAQ system is designed to be able to allow LED calibrations of the TPC PMTs in about 10 minutes. This requires an event rate of 4 kHz, resulting in a ~340 MB/s total waveform data rate. The fast (400+ MB/s for SSDs) storage drives in the individual DCs allow for sustaining such collection rates, and the amount of space offered by each DC permits significant buffering in case of connection problems to the off-site permanent storage, as shown in Table 11.5.3.

We are planning to use 7z compression. Nominally, 7z uses the LZMA algorithm, but we have found that the PPMd algorithm [4] is better suited for the waveforms we are going to collect. Based on comparisons made using LUX data, the 7z PPMd compression offered an additional 33% data reduction for waveforms and a 15% data reduction for reduced quantities over gzip, which was used in LUX.

Because the POD mode relies on time stamping, the entire DAQ system will run with a global 100 MHz clock. The DDC-32s, DEs, and DM will run with the external clock source. We are considering two ways

of distributing the clock, either by using a proven method of dedicated NIM logic clock FAN-IN/OUTs or using clock recovery from the serial links of the HDMI cables; the latter method is currently being evaluated. We are also looking at the possibility of using one of the single-ended channels of the HDMI cable for a dedicated clock signal.

The configuration, acquisition control, and monitoring will be done using the DECM workstation. For improved robustness, the DECM will communicate with all DAQ elements using an isolated 100/1000 LAN; the run-control (RC) system, described in Section 11.10, will not have direct access to the front-end digitizers. We have successfully tested and are planning to use ICE middleware as our communication framework [5].

11.6 Data Sparsification

The design of the LZ data sparsification system is based on our experience with event selection in the LUX trigger system. The top architecture of the LZ data sparsification system is shown schematically in Figure 11.5.1. The DAQ and data sparsification firmware operates in parallel on the FPGAs of the DDC-32 digitizers.

The DDC-32s continually process the incoming pulses and extract specific required quantities such as pulse area, pulse height, and time of occurrence. By using digital filters with various filter lengths, the system can distinguish S1 and S2 pulses. The parameters extracted from the waveforms by the DDC-32s are sent to the Data Sparsifiers (DSs) for further processing and generation of secondary quantities such as the multiplicity vectors of groups of PMTs and their total energy. These secondary quantities are sent to the Data Sparsification Master (DSM), where the final waveform selection decision is made. The decision to preserve the current waveforms is sent to the DAQ Master.

The LZ DAQ/Sparsification system is capable of handling event rates up to ~250 kHz. This is much higher than the highest event rates expected in the LZ detector, which will occur during LED calibrations (~4 kHz).

As in LUX, the PMT signals will be processed by parallel digital integrating filters, allowing for discrimination against area of the incoming pulses. The filter with an integration width of about 60-100 ns is tailored to S1-like pulses; the second filter with a few-microsecond width is optimal for wider S2-like pulses. The filters are designed to also perform automatic baseline subtraction.

As shown in Figure 11.5.1, the TPC, skin, and outer-detector PMTs will use separate DDC-32s and DSs because these PMTs have different purposes and the firmware will be tailored to their specific needs. Such separation also makes it easier to apply different scaling factors for the digitization of signals from different PMT groups. The three major waveform-selection modes for the central TPC PMTs are summarized in Table 11.6.1.

If a waveform selection condition is met, the DSM sends a signal to the DM. At the same time, a packet containing the selection parameters used to make the decision is merged with the captured waveform data. This allows for offline evaluation of the selection decision for every individual event. This feature has proved extremely valuable in monitoring LUX data quality.

Table 11.6.1. Summary of three major waveform-selection modes for the central TPC PMTs.

Trigger Mode	Summary
S1 Mode	Detection of coincident S1-like signals across selected channels. No fiducialization.
S2 Mode	Detection of coincident S2-like signals across selected channels. Fiducialization in the x,y plane.
S1 & S2 Mode	Detection of S1-like signals followed by S2-like signals within a selected drift time range. Fiducialization in x, y and z planes.

Similarly to the DAQ system, the DS system will be controlled and monitored by a dedicated DS expert control/monitoring (DSECM) workstation over an isolated 100/1000 LAN network. The DS system will operate on the same 100 MHz global clock as the DAQ.

The LZ DS system will adopt and expand on the monitoring capabilities of the LUX system. Capabilities such as performing continuous noise sweeps (monitoring S1 and S2 filter crossing rates as a function of threshold) or monitoring channel hit distributions of the selected events, all in parallel to regular uninterrupted data-sparsification operation, have been invaluable in LUX and surely will be in LZ.

Each of the DDC-32s has a dual 14-bit analog reconstruction output (SPY) allowing for diagnostics and scope monitoring. The SPYs can be sourced with individual incoming channels or their digital sum. They can also be sourced with S1 and S2 filter outputs, individual or summed, or any other signal internal to the FPGA. This feature will be very useful, especially in development and deployment stages, as proven in the LUX project.

11.7 PMT High-voltage Supplies

LZ will use the Wiener Mpod LX HV system to bias the Xe and the outer-detector PMTs. This system is currently being used for LUX. The system will provide negative HV to the Xe PMTs and positive HV to the outer-detector PMTs. The HV modules are part of the EDS 201-30x 504 series. Each module provides 32 HV channels and uses a common floating ground. The voltage ripple is less than 5 mV. The HV can be set with a resolution of 10 mV, and the current on individual channels can be measured with a resolution of 50 nA.

HV connections to the HV filters are made using Kerpen cable with Redel connectors on both ends. Each Kerpen cable carries HV for 32 channels. Important properties of the HV system are listed in Table 11.7.1.

Table 11.7.1. Details of the PMT HV system.

HV Module	Maximum HV	Max Current per Channel	PMTs	Channels	Required Number of Modules
EDS 201 30n	-3000 V	500 μ A	TPC/Skin	662	21
EDS 201 30p	+3000 V	500 μ A	Outer-detector	120	4

11.8 Cables

All network, signal, and HV cables are low smoke zero halogen (LSZH) cables. LZ uses the same cables that have been approved for LUX use in the Davis Laboratory. The exact lengths of the HV and the signal cables will be fixed once the location of the analog amplifiers is fixed and the route of the cable trays has been finalized.

The types of cable and their lengths are listed in Table 11.8.1. The networking cables will have various lengths; individual lengths will vary based on the location of the network switched and the location of the devices to be connected. About half of the network cables are used by the slow-control system; the other half will be used for the networks associated with the DAQ, trigger, and online systems.

We have not been able to identify a suitable HDMI cable that provides good performance and uses LSZH materials. The total length of these cables is small and the electronics racks are enclosed and vented directly into the exhaust system of the Davis Campus. This arrangement will be assessed by the SURF safety team. Note that rack enclosures and connections to the exhaust system are also used in LUX for this same reason.

Table 11.8.1. Information on LZ signal, logic, HV, power, and network cables.

Cable Type	Type	Length (ft)	Number of Cables	Notes
Network	Belden 7936A	10,000 (total)	750	Cat 6, LSZH, various lengths
Signal	LMR-100A-FR	56	128 bundles (8 cables/bundle)	LSZH
Logic	LMR-100A-FR	2	500	LSZH
HV	Kerpen	56	25	LSZH, 32 channels per cable
Power cords	CordMaster	6	100	LSZH
HDMI	TBD	TBD	99	Lengths TBD.

11.9 Slow Control

11.9.1 Requirements

Based on experience with LUX, we expect modest requirements for the bulk of the slow-control channels. For most channels, the rates will be less than 1 Hz and a latency of 1 s is acceptable. Typical data rates will be no more than a few kB/min/channel. The interfaces that will be used for most channels include the four-wire interface for the resistance temperature detectors (RTDs), analog inputs and outputs, relays, serial links (RS232 or RS485), and Ethernet links.

The hardware for these “standard” interfaces is included in WBS 1.8.5. Other interface types, not listed above, will be provided by the corresponding subsystem. The estimated requirements for the “standard” channels are summarized in Table 11.9.1.1.

Table 11.9.1.1. Slow-control interface needs.

WBS		RTD	Analog	Digital	Relay	Serial	Ethernet
1.3	LN system	20	14	10	10	21	14
1.4	Gas system					12	
1.4.1	Sampling	12	8	24	24	14	4
1.4.2	Kr removal	25	38	75	75	17	12
1.4.4	Delivery and recovery	30	23	12	12	31	4
1.4.5	Recirculation and purification	18	25	28	28	12	4
1.4.6	Liquid purification tower	20				10	
1.5	Detector		5			5	6
1.5.5	Xe system monitoring	100				10	
1.6	Veto	20	20				
1.7	Calibration		4	10	10	8	
1.8	DAQ and electronics	36	182			10	40
	Environment	40	10	10		5	5
	Total	321	331	169	159	155	89

11.9.2 Platform Choice

Not all the sensors/equipment monitored and controlled by the slow-control system are of the same importance. They can be broadly classified as “critical” sensors/equipment for which a failure or human error can damage equipment or result in loss of Xe, and “standard” sensors/equipment for which readout or control errors will not pose any immediate danger. We decided to use a hybrid platform, schematically shown in Figure 11.9.2.1, with an Allen-Bradley programmable logic controller (PLC) based system servicing the critical sensors/equipment. This system will be programmed using graphical ladder diagram language [6] — commonly used for implementing process control in industrial applications — to guarantee fast and reliable response in critical situations. The noncritical inputs and outputs will be serviced by a database-centered system. The interface between the PLC and the database will be implemented using SQL bridge [7]. Such an approach allows us to minimize the slow-control system cost without compromising its reliability. As an additional safety feature, a standalone emergency system will provide redundancy, taking control over critical hardware in the unlikely case of a PLC failure.

The noncritical system is built around the main slow-control database that serves as a hub between the slow-control core, device drivers, and the user interface. The core is very compact and lightweight. The hardware-specific device drivers transfer the information between the hardware devices and the database. It is important to note that the drivers run as separate processes, and the system as a whole remains stable if one of the drivers fails. Hot-swapping the drivers is not a problem either. The components of the system can be distributed across different computers or even different hardware platforms; e.g., part of the drivers can run on an embedded system if necessary. The safety of operation is ensured by two constantly running pieces of software: the main watchdog that is responsible for starting, stopping, and monitoring hardware drivers, and the alarm system, which constantly monitors the critical parameters and alerts all interested parties if they go outside a predefined range.

The database is constantly mirrored to a separate computer in the Davis Laboratory and to several computers on the surface. Underground access to the database is configured for high availability [8], with the primary mirror seamlessly taking over from the master database in the case of problems or required maintenance. The slow-control software also uses an ICE server for direct communication with run control (RC) (see Section 11.10.1). Through this server it is possible to monitor and control a limited number of important parameters, bypassing the database. This additional redundancy increases the overall

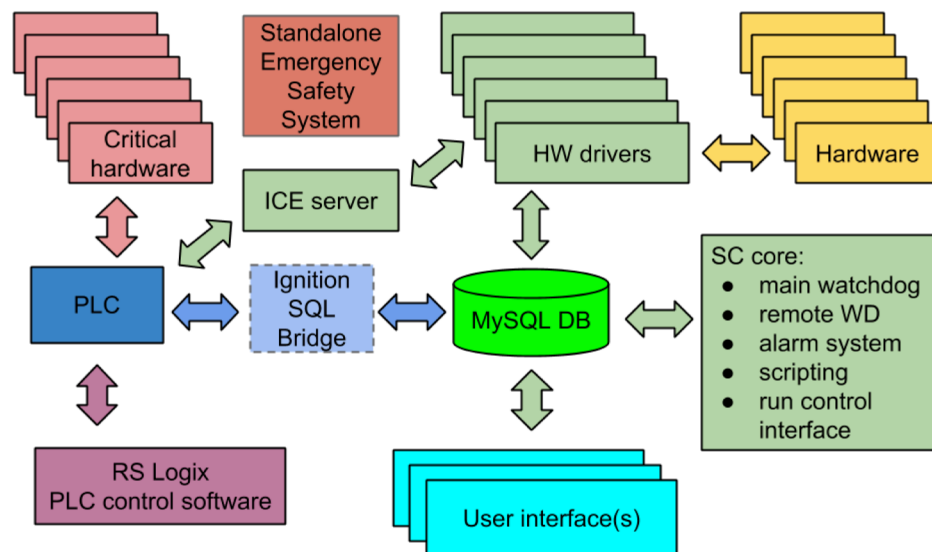


Figure 11.9.2.1. Slow-control functional diagram.

robustness of the system in critical situations.

The noncritical control and monitoring software will be based on the open-source slow-control system developed for and currently used by LUX. This choice is based on several factors. The LUX system can be easily scaled up to the expected number of channels and data rate for LZ. From a safety point of view, it is very robust due to its modular architecture and is designed to provide quick response in emergency situations. An important additional factor is the existing level of experience in the collaboration.

11.9.3 Special Requirements

According to our estimates, the platform described above will be able to handle up to a few thousand standard channels (<1Hz, >1s latency) without overload. These rate and latency limits are not strict, but are guidelines to guarantee that all the channels play “nicely” together in the large system.

A small fraction of channels are expected to go beyond the standard requirements. For example:

- The temperature and pressure sensors in the circulation and Kr removal subsystems
- The valves for Kr injection
- The nonstandard sensors related to the Xe vessel and TPC: acoustic, radio, and camera

Faster readout and control (~10 Hz, ~0.1 s latency) for a limited number of channels is not a problem even for the base system. If faster acquisition (up to few kHz) is required, the solution would be a dedicated acquisition board with an embedded Linux system running a slow-control hardware driver. The data will be stored in a dedicated database to reduce the load on the main system. Such an add-on can be seamlessly integrated into the main slow-control system due to the modular design of the latter.

11.9.4 Network

The Ethernet network (Figure 11.9.4.1) is the backbone of the slow-control data flow. For this reason, a high-performance local network is built on site. Each subsystem is equipped with a dedicated managed switch and a number of unmanaged switches if necessary. All the “standard” interfaces are ultimately routed through an Ethernet link: via ADAM modules for RTDs, analog input/output, and relay controls; and via serial-to-Ethernet adapters for RS232 and RS485. The subsystem switches are linked to the main 48-channel managed switch connected to the main slow-control computer via a gigabit uplink. The cabling will be made with LSZH cables, ensuring triple redundancy for the links to the main subsystems.

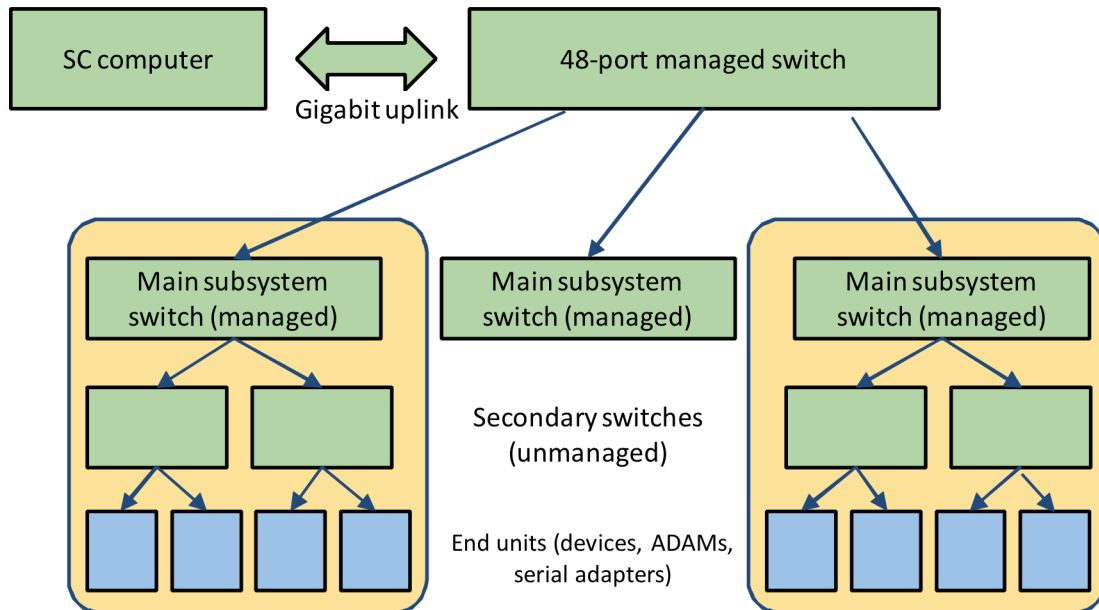


Figure 11.9.4.1. Slow-control system network.

11.10 Online System

The core of the online system is the run-control system (RC), schematically shown in Figure 11.10.1. It comprises the software and hardware required to allow the operator to define and initiate data collections of different types, control and monitor subsystems (DAQ, slow control, EB, and offline software), and log key information to the database. The physical system is hosted on a single rack-mount computer, identical to the hardware used for the event builder. The use of identical hardware with an on-site spare minimizes any downtime of this critical system. RC software is maintained on a mirror system throughout the project and operation periods to allow off-line debugging and code development.

The work on the RC system started with defining the architecture of the system and the development of detailed specifications and interface documents with the various subsystems. An important decision was the selection of the middleware to be used for communications between RC and the subsystems. We have past experience with a number of middleware packages, in particular the industry-standard CORBA (Common Object Request Broker Architecture) system. Given the limitations of CORBA, e.g., scalability, throughput, reliability, and thread-safety, a new solution was considered with similar functionality but improved performance. A recent study [9] to identify middleware to run CERN accelerators ranked ICE (Internet Communications Engine) and ZeroMQ as the top two evaluated systems. The criteria for this evaluation included reliability and speed, and the ability of the system to handle a large number of messages per second (both small and large messages) and publish to a large number of clients in minimal time. Based on preliminary comparisons ICE has been identified as the best choice for LZ middleware. ICE is an object-oriented system similar to CORBA, but improves on many of CORBA's limitations. ICE provides both a request-reply and publish-subscribe service. ICE supports C++ calls and runs on Linux. The RC software will be developed using a combination of C++ and Python, and run on a Linux-based server. We have not yet selected the final graphics/GUI (graphical user interface) library, but PyQt [10] appears to be the most promising and will be the basis of our initial development. To make our code somewhat independent of the specific choices for the system architecture, a library of wrappers will be developed for various low-level system calls, including

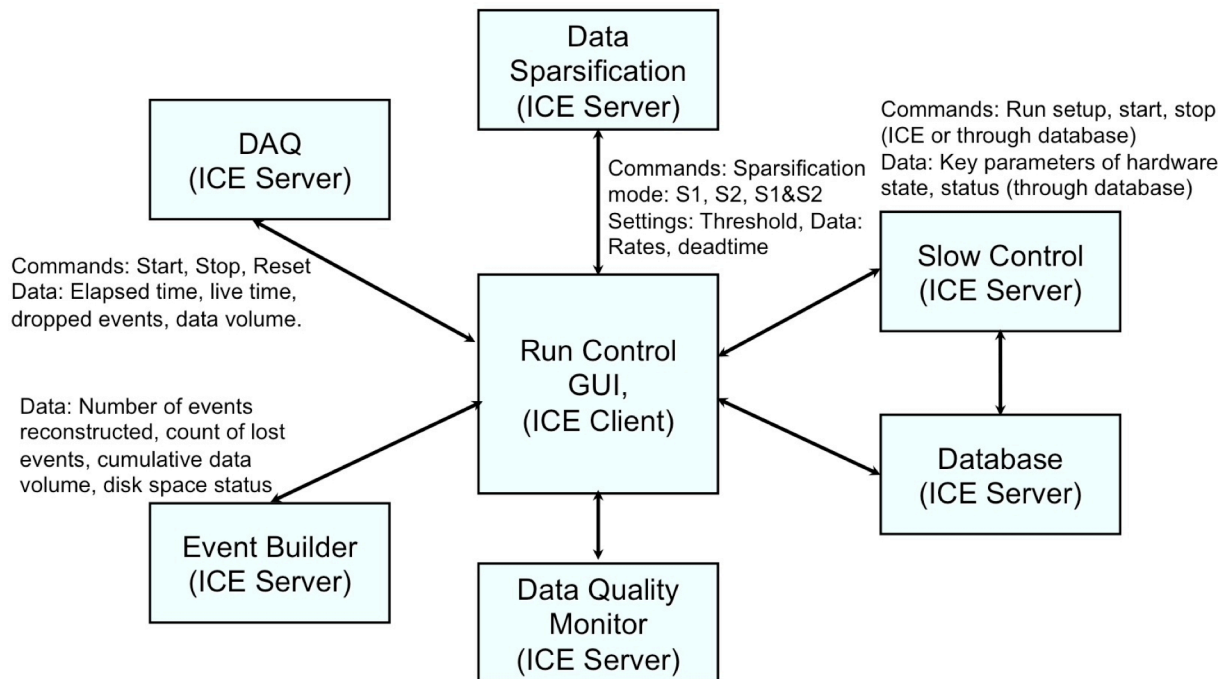


Figure 11.10.1. Block diagram showing the primary interfaces between the RC system and other LZ subsystems. The users use a GUI to interact with the RC system.

common command/control interfaces, database queries, and graphical display/plotting commands.

To provide a seamless interface to the DAQ system, each data collection mode (e.g., calibration runs, data runs) is associated with a corresponding set of command sequences to the various subsystems. The list of data collection modes includes normal data-taking modes (S1 only, S2 only, S1 and S2; see Table 11.6.1 for more details) and a number of calibration modes, including the LED, krypton, tritium, and neutron calibration (see Chapter 10 for more details). The RC group will interact closely with the groups responsible for the various subsystems to determine the required interfaces, including defining what status information is shown, what commands are provided, and how status information should be displayed. Based on this information, the RC group will develop an application programming interface (API) and skeleton (server/daemon) program for each subsystem, including the appropriate handles for communication with RC, covering commands and sharing of status information. These skeleton server programs will be further developed by each group for their specific subsystem, working in close consultation with the RC programmer. This model has worked very well in the past, expediting code development compared with the model in which each subproject is expected to develop its own interface code from scratch.

Throughout the course of the development, the run-control and slow-control groups will work together closely and try to adhere to common standards for coding, code-management, and common libraries for communication and interfaces. Most data sharing between run-control and slow-control will occur through the database, but some of the most important commands will occur through a direct ICE connection between slow-control server computers and the run-control system.

The final RC system provides the user with a simple GUI to the DAQ, data quality monitoring, and the slow-control systems. The GUI will guide the user through setting up and starting/stopping various data-collection modes and starting runs, making sure all settings, data, and operator comments are logged into the database. The GUI includes key alerts for out-of-bound values, as determined by the slow-control system, and provides a small number of user-selected plots that allow the user to quickly monitor the health of the LZ system.

A skeleton version of the RC software will be developed for the electronic system test. During this development period, the options for the basic system framework will be determined and the system hardware will be purchased. The RC group will work with software developers for the other subsystems to develop interface control documents (ICDs) specifying command sequences, settings, and critical data to be exchanged directly through an ICE link or indirectly through the database. Lessons learned from the electronic system test and the feedback from early users will provide input for the final design phase, during which ICDs will be finalized and the full set of interfaces between RC and the subsystem implemented.

Because the code will be developed and maintained by an experienced professional programmer, it is expected that the RC system will be well maintained throughout the LZ project and operation periods, with minimum downtime.

11.11 Installation

The electronics will be installed in two locations. The analog electronics for the Xe PMTs will be installed on the mezzanine level, as shown schematically in Figure 11.11.1. The amplifiers will be arranged in eight to 10 racks, with 10 amplifier cards installed in each rack. The racks will be located horizontally on the wall of the water tank in order to improve cooling and provide better access to each amplifier crate. Exhaust ducts may must be installed at this location to facilitate cooling of the electronics. Because it will be difficult to enclose the electronics crates at this location, it is important the air flowing over the electronics is directed into the exhaust system. This will prevent any smoke generation as a result of an electrical problem, e.g., overheating of components, from spreading into the Davis Campus. The

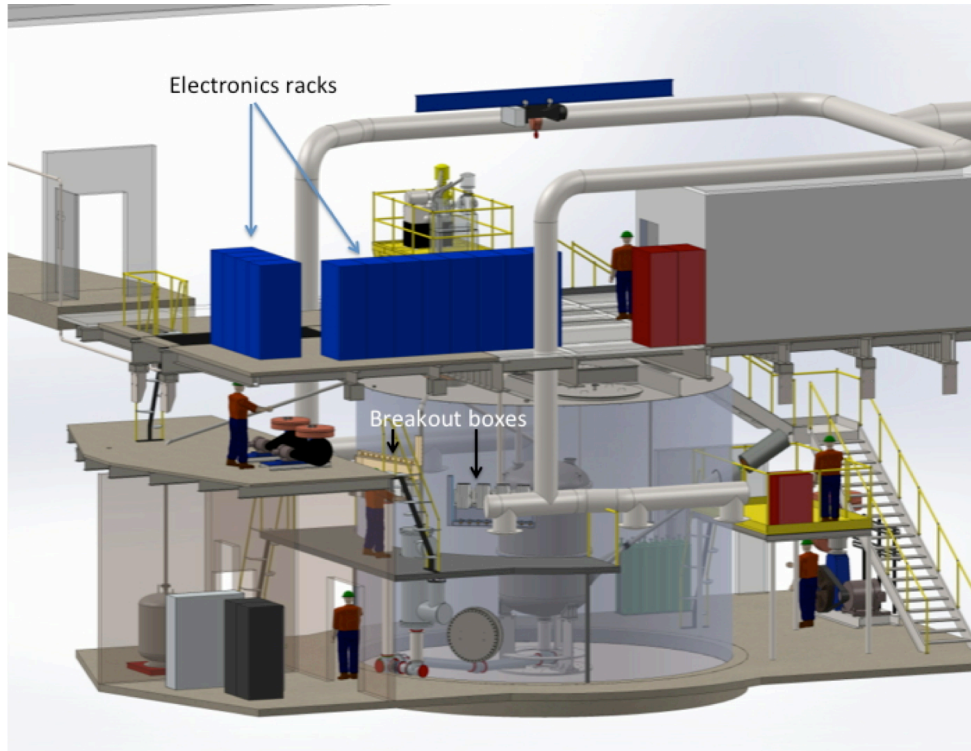


Figure 11.11.1. Installation of the analog electronics for the Xe PMTs at the mezzanine level and the electronics racks at the deck level.

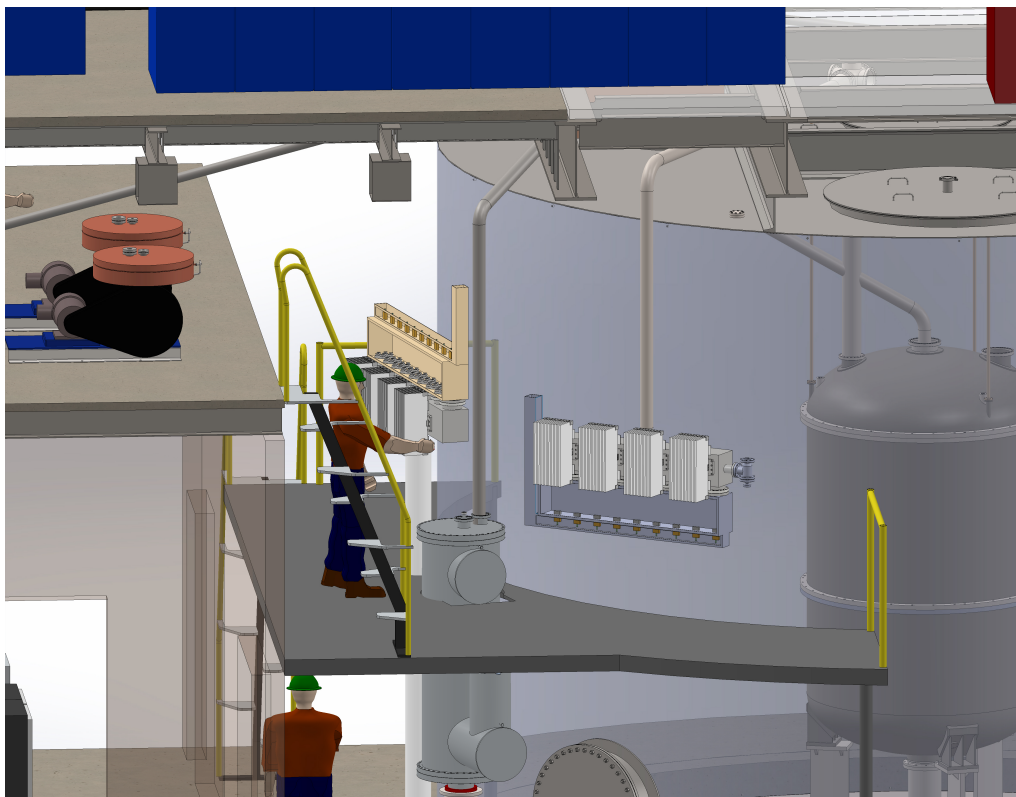


Figure 11.11.2. Close-up of the mezzanine level showing the amplifier racks installed on the breakout boxes.

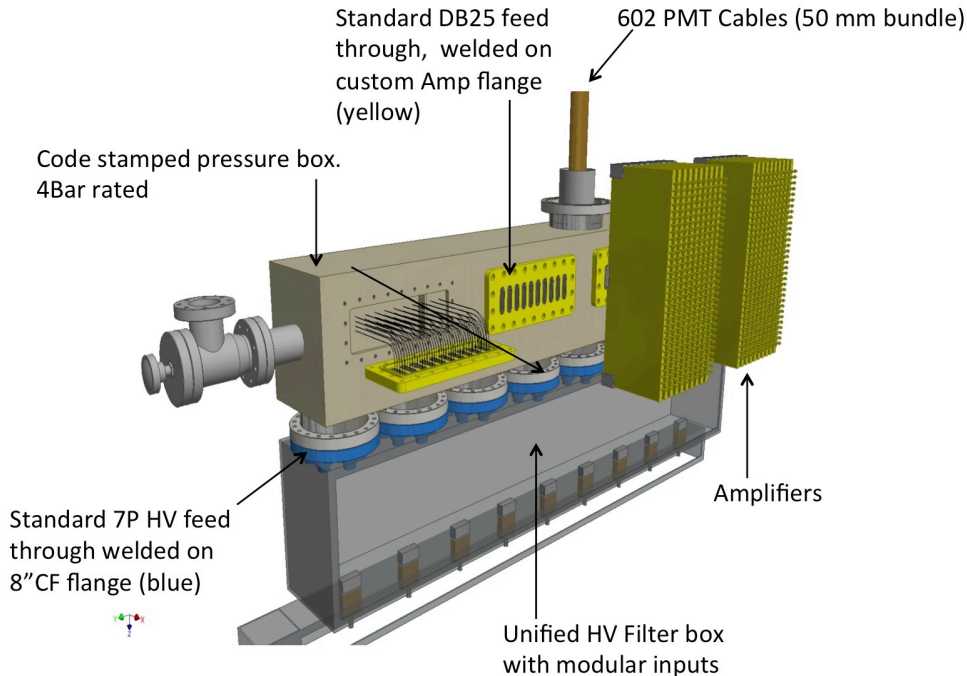


Figure 11.11.3. The breakout box for the PMTs located in the top of the cryostat. Two electronics crates with 10 amplifiers each are attached to two flanges on the breakout box. The grey box, mounted below the pressure box, contains the HV filters. The location of the breakout boxes is shown in Figure 11.11.1.

outputs of the amplifiers are routed in cable trays to the DAQ and trigger systems installed in the electronics racks installed at deck level (see Figures 11.11.1 and 11.11.2).

A schematic of the breakout box, with the amplifier racks disconnected from the box, is shown in Figure 11.11.3. The internal signal and

HV cables enter the breakout box through the conduit at the bottom of the box. The signal cables are routed to the rectangular DB-25 connectors on the rectangular flanges with the amplifier crates. The HV cables are routed to the round HV flanges, visible on the top of the breakout box.

The amplifiers and the HV pickoffs for the outer-detector system will be installed in the electronics racks shown in Figure 11.11.1. The HV cables from the outer-detector PMTs are routed via one of the flanges on top of the water tank to this location. The design of the flange is such that no connectors are required to ensure a light-tight and radon-

Table 11.11.1. LZ power requirements in the Davis Laboratory

System	Predicted load (kW)	Maximum load (kW)
Thermosyphon tower	4.2	4.2
Circulation panel	7.9	7.9
Storage panel	0.1	0.1
Storage system	10.9	10.9
Emergency control	0.5	1.5
LN ₂ storage	22.6	22.6
Gas control	1	1
Breakout carts	4.6	4.6
Amplifiers	4.8	12
DAQ	30.5	42
Data Sparsification	20	24
Monitoring computers	2.1	6
HV and slow control	12.5	23
Ultrasonic cleaning	2.3	2.3
Water system	13.1	13.1
Control room	5.8	5.8
Tools	1.3	1.3
Total	146	188

tight connection. Not using connectors on the flange improves signal quality.

A total of 12 electronics racks are installed at the deck level, as shown in Figure 11.11.1, to provide space for all electronics systems, except the Xe amplifiers, and the computer and disk systems. The racks are fully enclosed and the forced airflow across the electronics is directed into the exhaust system of the Davis Laboratory.

The power requirements of the electronics system in the Davis Laboratory have been estimated and are summarized in Table 11.11.1. These estimates are based on the measured power consumptions of the various components of the system. The maximum load is the load of the equipment at startup. The power required by the electronics systems is provided by uninterruptible power supplies installed in the electronics racks. The total maximum load of the electronics is 109 kW.

Table 11.11.1 also shows the power consumption by other LZ systems.

Chapter 11 References

- [1] *All Programmable FPGAs and 3D ICs*, Xilinx Inc., 2100 Logic Drive, San Jose, CA 95124-3400, USA (2015).
- [2] D. S. Akerib *et al.*, *Nucl. Instrum. Meth.* **A668**, 1 (2012), arXiv:1108.1836 [astro-ph].
- [3] E. Druszkiewicz, *Digital Advances in Triggering and Data Acquisition Systems for Large Scale Dark Matter Search Experiments*, Ph.D. thesis, University of Rochester (2015), [manuscript in prepration].
- [4] D. Salomon and G. Motta, *Handbook of Data Compression* (Springer London, 2010) ISBN 978-1-84882-902-2.
- [5] M. Henning, *IEEE Internet Computing* **8**, 66 (2004).
- [6] A. Crispin, *Programmable Logic Controllers and Their Engineering Applications* (McGraw-Hill, 1997) ISBN 978-0-07709-317-4.
- [7] *Ignition SQL Bridge*, Inductive Automation, 340 Palladio Parkway, Suite 540 (4th Floor) Folsom, CA 95630-8833, USA (2015).
- [8] B. Schwartz, P. Zaitsev, and V. Tkachenko, *High Performance MySQL: Optimization, Backups, and Replication*, 3rd ed. (O'Reilly Media, 2012).
- [9] A. Dworak, P. Charrue, F. Ehm, W. Sliwinski, and M. Sobczak, in *13th International Conference on Accelerator and Large Experimental Physics Control Systems, 10-14th October 2011, WTC Grenoble, France* (2011) pp. 1334–1337, *Middleware Trends And Market Leaders 2011*.
- [10] *PyQt*, Riverbank Computing Limited, Redcotts House, 1 Redcotts Lane, Wimborne, Dorset BH21 1JX, UK (2015).